The Pennsylvania State University

The Graduate School

College of Earth and Mineral Sciences

THE EFFECTS OF THERMAL CYCLING ON THE PERMEABILITY AND MECHANICAL PROPERTIES OF SHALE

A Thesis in

Energy and Mineral Engineering

by

Brandon A Schwartz

© 2016 Brandon A Schwartz

Submitted in Partial Fulfillment
of the Requirements
for the Degree of

Master of Science

December 2016

The thesis of Brandon A Schwartz was reviewed and approved* by the following:

Derek Elsworth
Professor of Energy and Geo-Environmental Engineering
Thesis Adviser

Shimin Liu
Assistant Professor of Energy and Mineral Engineering

Chris Marone
Professor of Geosciences

Sanjay Srinivasan
Professor of Petroleum and Natural Gas Engineering
Interim Associate Department Head for Graduate Education

*Signatures are on file in the Graduate School.

Abstract

The feasibility and rate of recovery of natural gas from tight shale formations is controlled by matrix permeability and flow path length to the closest permeable conduit (fracture). The purpose of this study is to understand the evolution of transport (∂k) and mechanical (∂K) properties of shale due to applied static and cyclic thermal (∂T) stimuli. We report the evolution of permeability and bulk modulus in shales under static and cyclic thermal loading. Experiments were conducted on core samples under recreated in situ conditions. All experiments retained total stress and pore pressure constant to isolate the response of permeability and bulk modulus due to thermal stimuli, alone. Experiments were on both fractured and unfractured samples to understand the respective susceptibilities of fracture and matrix permeabilities to thermal loading. We show that before fracture coalescence permeability has a direct relationship to temperature and an inverse relationship to bulk modulus. Both permeability and bulk modulus show an hysteretic nonlinear response to thermal cycling. Permeability evolution in both fractured and unfractured samples is similar, although differences include the magnitude of permeability enhancement and the effect of matrix compaction on permeability. Deformation data suggest that thermal stress can reactivate primary consolidation. Based on experimental data, we propose a model that links permeability evolution as an inverse function of changes in bulk modulus.

Tables of Contents

List of Figures

Acknowledgements

I want to thank my advisor Dr. Derek Elsworth for his mentorship and guidance throughout this study, as well as Dr. Chris Marone for providing me direction with my experimental data. I want to thank Chevron for their generous financial support, as well as their insight and feedback throughout the project.

Author
Brandon A. Schwartz

Chapter 1: Introduction

Both permeability and rock stiffness change with temperature (Closmann 1979, Zhu 2013). However, the relationship between these two properties under thermal loading and for shales is largely unknown. Few studies have been conducted to measure thermally induced permeability and the evolution of rock stiffness in shale. Shale basins are known to contain natural hydraulic fractures, but the relationship between fracture permeability and matrix permeability remains poorly understood. The following summarizes current understanding of the roles of thermal effects on the permeability and deformability of shales, including the key role of sorption.

There are several competing mechanical processes in sorptive media. There are mechanical stresses caused by the overburden stress and the pore pressure. With sorptive rocks there is the additional effect of organic swelling. This has been reported to cause a permeability reduction in coals and to a lesser degree in shales (Kumar 2015). Permeability reduction is controlled by crack geometry, Langmuir swelling, and void stiffness, whereas permeability enhancement is controlled by crack geometry and void stiffness alone (Izadi 2011).

When thermal effects are considered the competing processes become more complex. Increased temperature causes organic matter to shrink as gas desorbs, resulting in fracture dilation (Levine 1996). An increase in temperature also causes mineral expansion of rock bridges across fractures – resulting in an increase in fracture aperture. The relationship between permeability and temperature in coal is dependent on whether the thermal stress is larger than the external stress (Yin 2013). An increase in temperature has been reported to cause permeability reduction in shales although the underlying mechanism was not determined (Sinha 2013).

Many permeability models for sorptive media have been proposed (Liu 2011, Palmer 2009). Among the most utilized are the P&M model, the Shi-Durucan model, the ARI model, and the Izadi model. The Shi and Duracan (S&D) model is similar to the P&M model with the exception that it is stress dependent rather than strain dependent and assumes a constant pore volume compressibility (Shi and Duracan 2005). The ARI model assumes the internal strain is proportional to the gas concentration (Pekot 2003). Additional characterizations of permeability evolution in coals (Chen 2012, Wang 2012, Wu 2011, Liu 2010) account for internal swelling and consider fracture-matrix interactions (Liu et al 2010).

Both permeability and rock stiffness are influenced by microcrack density. Microcrack growth is controlled by local tensile stresses generated by grain mismatch and irregular grain boundaries (Costin 1983). Microcracks coalesce after sufficient crack propagation (Eberhardt 1999). Laboratory tests on European black shales show that rock stiffness decreases with increasing temperature in single stage uniaxial compression tests (Rybacki et al 2015). Thermal stimuli can lead to increased permeability due to microcracks coalescing in the rock fabric (Faoro 2013).

The relationship between rock stiffness and permeability in shales remains poorly understood. The response of fractures in shales under thermal loading remains largely unknown. Inelastic effects are often ignored in permeability models and require further study. Here we present laboratory results to explore the response of permeability and rock stiffness in fractured and unfractured shale cores under static and cycle thermal stress.

Chapter 2: Methodology

With anticipated important influences due to sorption and stresses, the evolution of deformability and permeability evolution is measured in response to static and cyclic thermal stresses under recreated in situ conditions. The experimental suite examines the evolution of both fracture and matrix permeabilities and ensemble deformability, and their relative susceptibilities to thermal loading.

2.1 Experimental Setup

Experiments were performed in a triaxial cell with three positive displacement pumps used to create confining pressure, axial pressure, and pore pressure. To capture sorptive and nonsorptive effects, methane and helium were used as saturants and permeants. Piezoelectric transducers (PZTs) were used to capture acoustic data. An LVDT was used to capture longitudinal deformation. The triaxial cell was placed into an insulated oven capable of regulating temperature up to 150^{o}C. Pressure pulse tests were used to measure permeability (Brace, 1968). Pore pressures were kept constant throughout the sample when permeability tests were not being performed. Experiments were conducted on a 3 mm thick fractured sample (Figure 2.2) and a 26 mm thick unfractured sample, both of which were 19 mm in diameter. Both samples were cored perpendicular to bedding planes. Samples were allowed to consolidate before testing. The rate of consolidation slowed after approximately 12 hours (Figure 2.3).

Figure 2.1: Schematic of experimental setup.

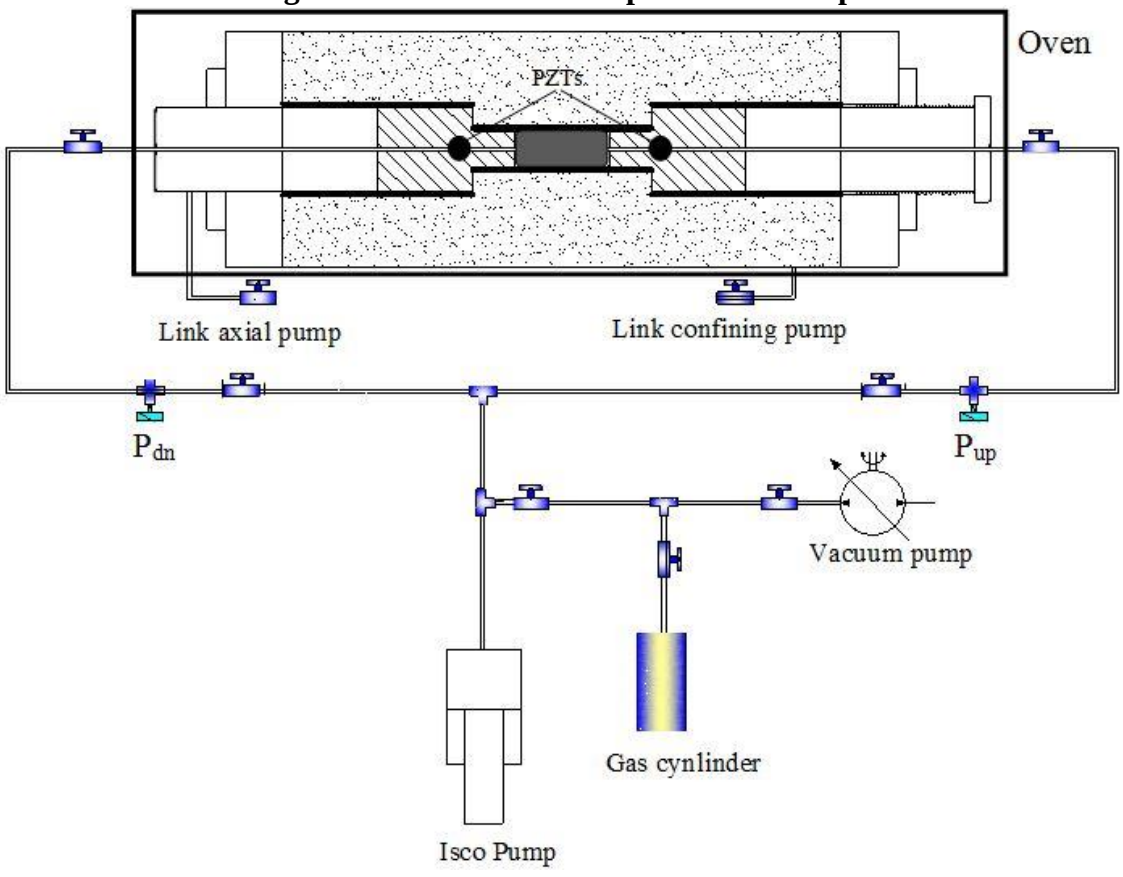

Figure 2.2: Sample with through-going fracture.

2.2 Experimental Methodology

Measurements were begun at room temperature. After permeability was measured at different pore pressures, the temperature of the oven enclosing the pressure cell would be raised to the next temperature set point. The temperature range tested was 23°C to 50°C for the fractured sample and 35°C to 65°C for the unfractured sample. Both temperature ranges were chosen to explore low amplitude thermal stimuli near the reservoir temperature. The first experiment was designed to capture static thermal effects when gas flow was predominantly through a fracture. The second experiment was designed to explore cyclic thermal effects through an unfractured sample in order to capture matrix dominant mechanisms.

In the experiments with the fractured sample, methane and helium were used as the permeant. Axial and confining stress were kept constant at 30 MPa. After completing a set of permeability tests with methane, the sample was vacuumed until the methane was removed and the experiment was repeated with helium. Permeability was measured at 1 MPa increments in pore pressures. After completing each set of permeability measurements at equilibrium temperatures, the temperature of the oven would be raised. Permeability measurements were made at 23°C, 30°C, 40°C, and 50°C.

In the experiment with the unfractured sample, axial and confining stress were kept constant at 24 MPa while the pore pressure was kept constant at 6 MPa. The pore pressure was only perturbed when pressure pulse tests were performed once per day. During pressure pulse testing the upstream pressure was raised to 6.5 MPa and the downstream pressure was lowered to 5.5 MPa. The sample was allowed to consolidate for six days before testing. Temperature was cycled at four set points: 35°C, 45°C, 55°C, and 65°C. At each pressure pulse test, acoustic data was gathered and the travel times for the p-wave and s-wave were converted to dynamic bulk modulus. Three cycles were completed and temperature, deformation, acoustics, and permeability were recorded. The last two data points for the third cycle—45°C and 35°C—could not be captured due to an equipment malfunction at the end of the experiment.

Figure 2.3: Deformation versus time for a 3 mm thick sample showing reduction in compaction rate. Negative deformation is compaction.

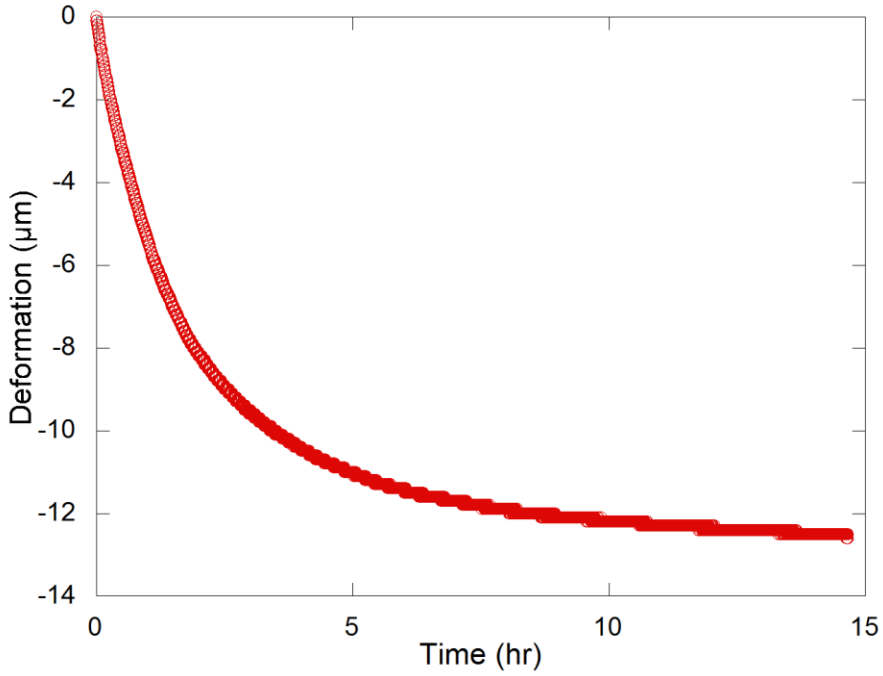

Chapter 3: Results

Observations are presented from experiments measuring the evolution of permeability and deformability (unfractured only) to thermal stresses in both fractured and unfractured samples of shale. Deformation measurements during cyclic thermal loading examine the potential for thermal stresses to reactivate primary consolidation and thereby influence permeability.

3.1 Fractured Sample Experiment

The permeability of the fractured sample was measured and shown to be of the order of 10^{-18} m^2. All results are normalized as a ratio of the measured permeability to a datum permeability, which was taken to be the first measurement at 1 MPa. Each subsequent plot presents a k/k_0 of unity at 1 MPa. As apparent in Figure 3.1, the permeability of the fractured shale sample exhibits the same inflection signature with increasing pore pressure as is reported in the coal literature. The methane gas curve shows a much larger reduction in permeability—a 50% drop—than the helium gas curve, which never falls below 80% of the reference measurement. Helium measurements should have only captured poromechanical expansion. The drop in helium permeability may be indicative of a high creep rate.

Figure 3.1: Permeability evolution of methane and helium as a function of changing pore pressure. External stress is constant and hydrostatic at 30 MPa.

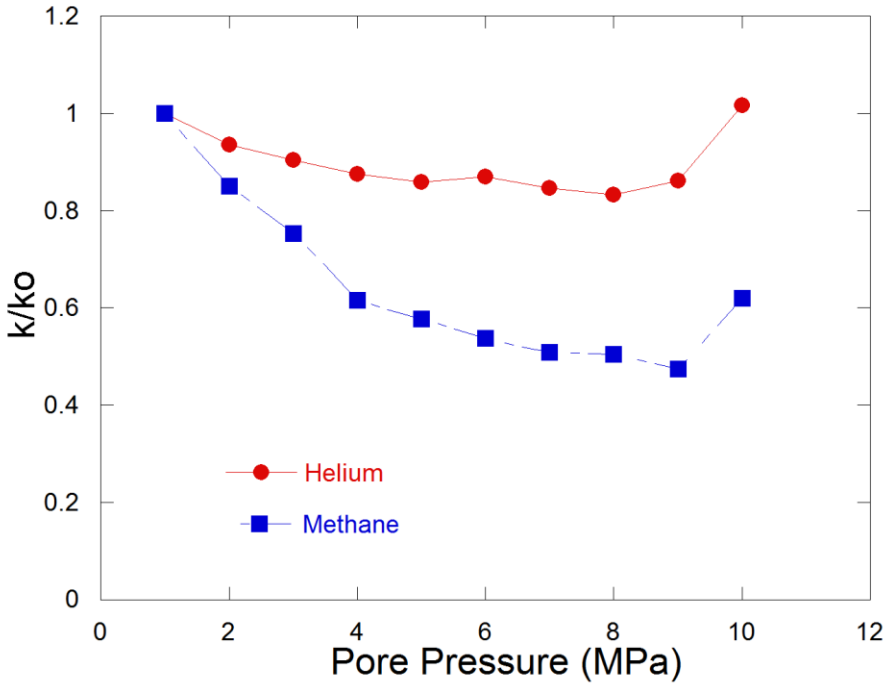

Deformation data were recorded and converted to strain. Figure 3.2 shows the change in strain from a datum measurement taken at 1 MPa for each gas (therefore each $\Delta\varepsilon$ plot begins at zero). The difference in strain between the methane and helium observations is due to sorptive strain. After the pore pressure reached 3 MPa the strain during the methane measurements became increasingly larger than the strain in the helium measurements. In Figure 3.3, change in permeability is plotted as a function of change in strain.

Figure 3.2: Change in strain as a function of pore pressure.

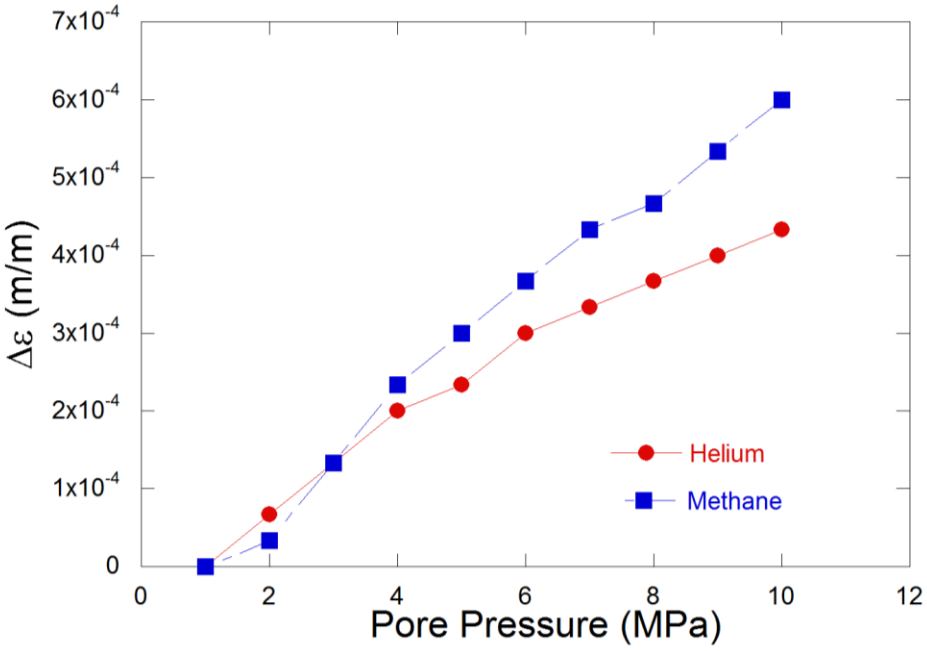

Figure 3.3: Permeability evolution as a function of change in strain.

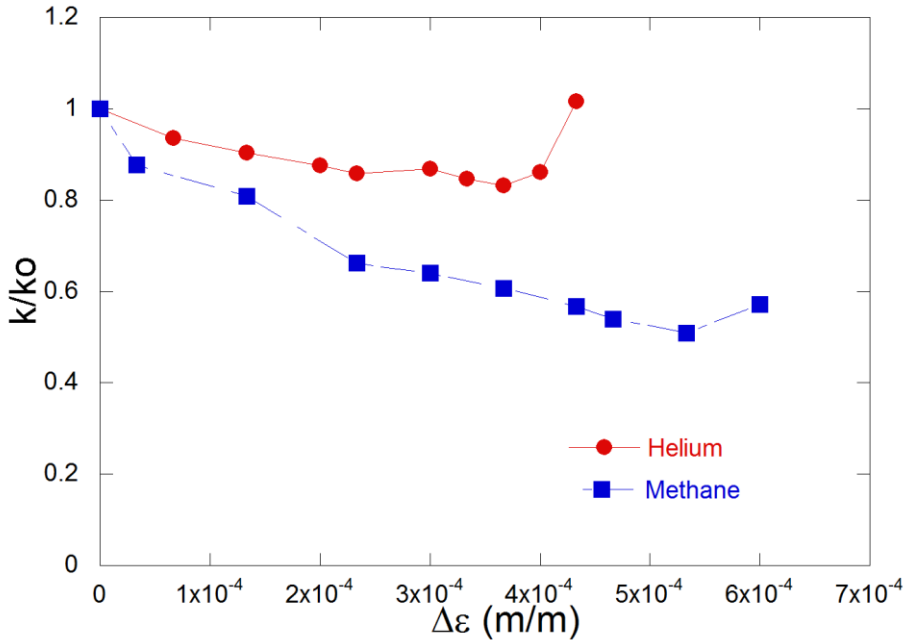

Figures 3.4 and 3.5 show the permeability to each gas plotted as isotherms. It is apparent that the permeability signature of each gas did not change with temperature. In both gases the final pore pressure measurement shows that permeability rebounds at 23°C and 30°C, but continues permeability reduction at 40°C and 50°C. This is likely due to a time effect such as creep or additional consolidation due to compressive thermal stresses causing the sample to retrace an additional part of its stress history. Isobars of permeability as a function of temperature are plotted

in Figure 3.6 and Figure 3.7 for methane and helium respectively. There is a generally increasing permeability trend observed in the isobaric data.

Figure 3.4: Methane permeability isotherms as a function of increasing pore pressure.

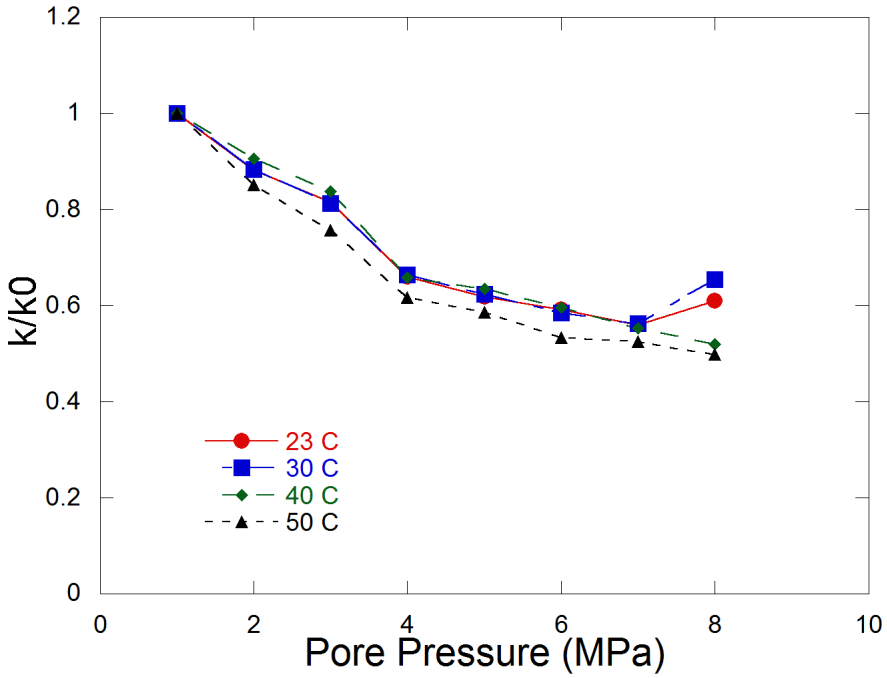

Figure 3.5: Helium permeability isotherms as a function of increasing pore pressure.

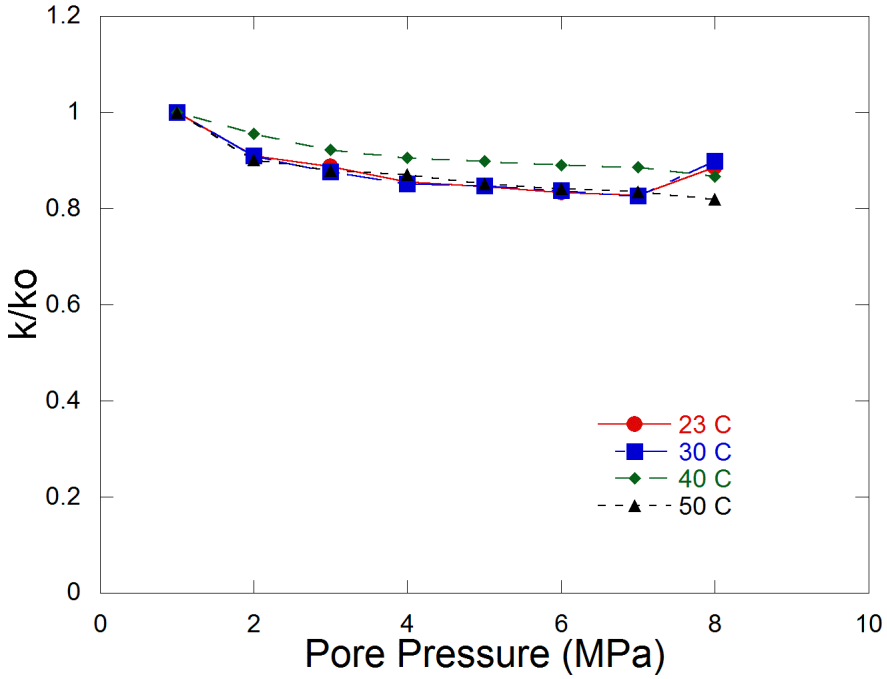

Figure 3.6: Methane isobars showing permeability as a function of temperature.

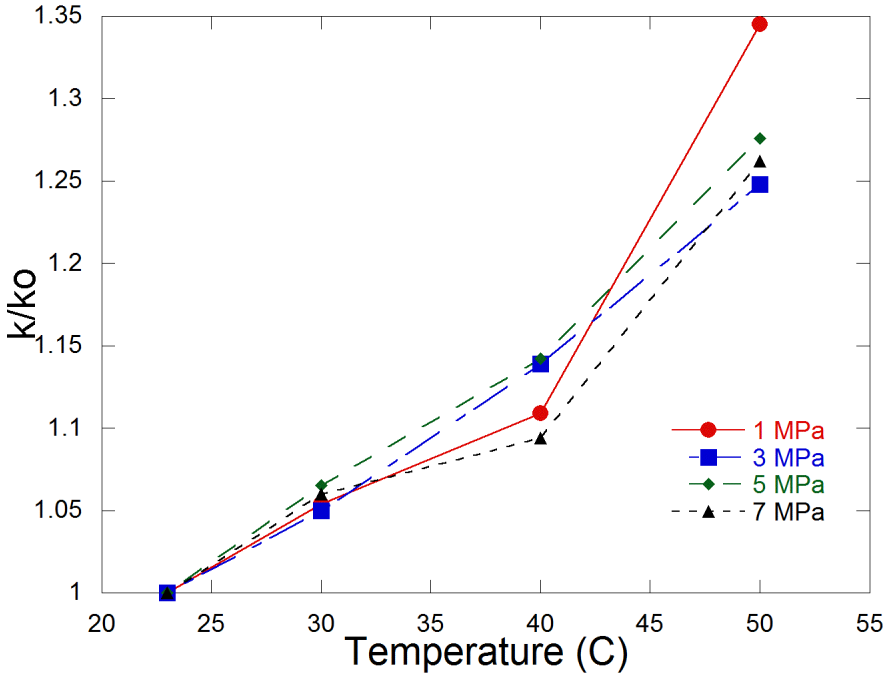

Figure 3.7: Helium isobars showing permeability as a function of temperature.

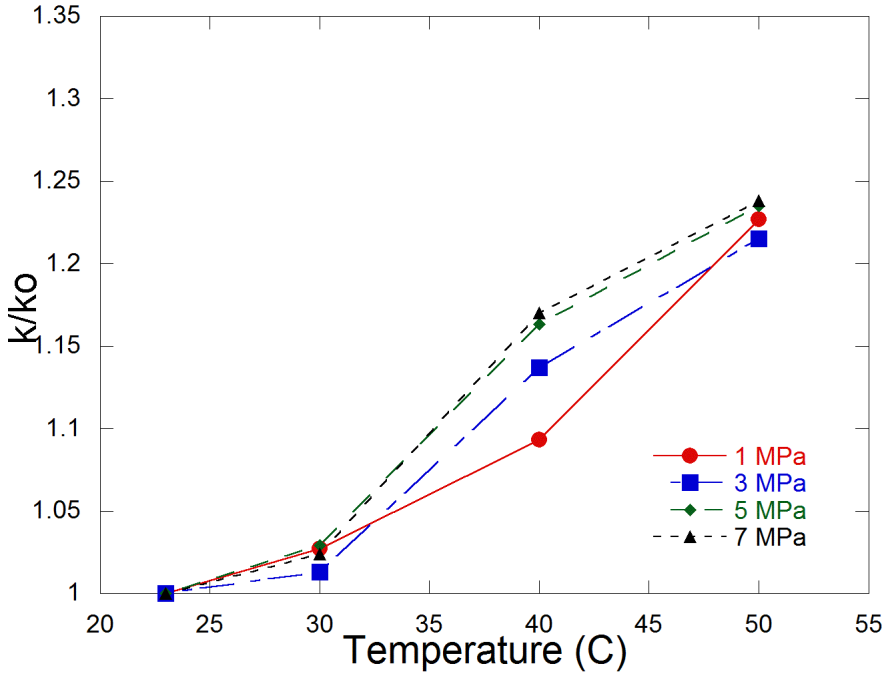

3.2 Unfractured Sample Experiment

In the second experiment, temperature cycles were conducted on an unfractured sample. All permeability values were of the order of 10^{-21} m^2. The sample was retained at constant hydrostatic stress of 24 MPa with a 6 MPa pore pressure throughout the experiment. Permeability was normalized relative to the permeability after five days of compaction. Figure 3.8 shows the permeability results along with the temperature cycles. There was an approximate 50% loss in permeability during the first cycle. The second cycle saw a permeability rebound as temperature was increased, consistent with the results from the first experiment with the fractured sample. Upon thermal unloading this permeability increase was reversed. The third cycle shows a similar trend.

Figure 3.8: Permeability vs. time and temperature vs. time for three thermal cycles.

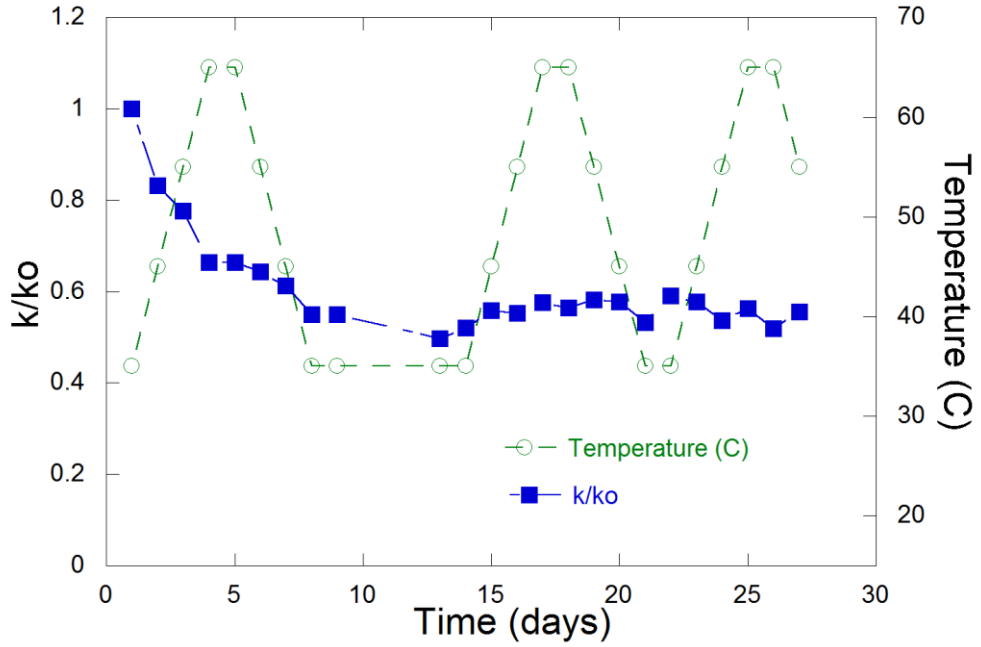

Figure 3.9 shows the evolution of the bulk modulus recovered from V_p measurements. There was a slight decrease in bulk modulus during the initial thermal loading at the beginning of the first cycle. The modulus experienced a 27% increase upon cooling. During the second cycle, the measured bulk modulus decreased with increasing temperature. Upon cooling, the measured bulk modulus increased. The third cycle shows a similar trend.

At the beginning of the experiment, the sample consolidated for five days at 27°C until it entered a slow creep rate. However, as Figure 3.10 shows, the first heating phase caused an additional strain that resulted in a 0.47% compaction that was not recovered upon cooling. As can be seen by the deformation patterns in subsequent cycles, the deformation data reached a mostly elastic response to cycling with temperature after this initial loss of length. The LVDT captured thermal expansion of the shale and the steel triaxial cell. The 0.1233 mm of unrecovered deformation is attributed to the 26 mm shale sample. Figure 3.11 compares the change in permeability to the change in bulk modulus.

Figure 3.9: Bulk modulus vs. time and temperature vs. time for three thermal cycles.

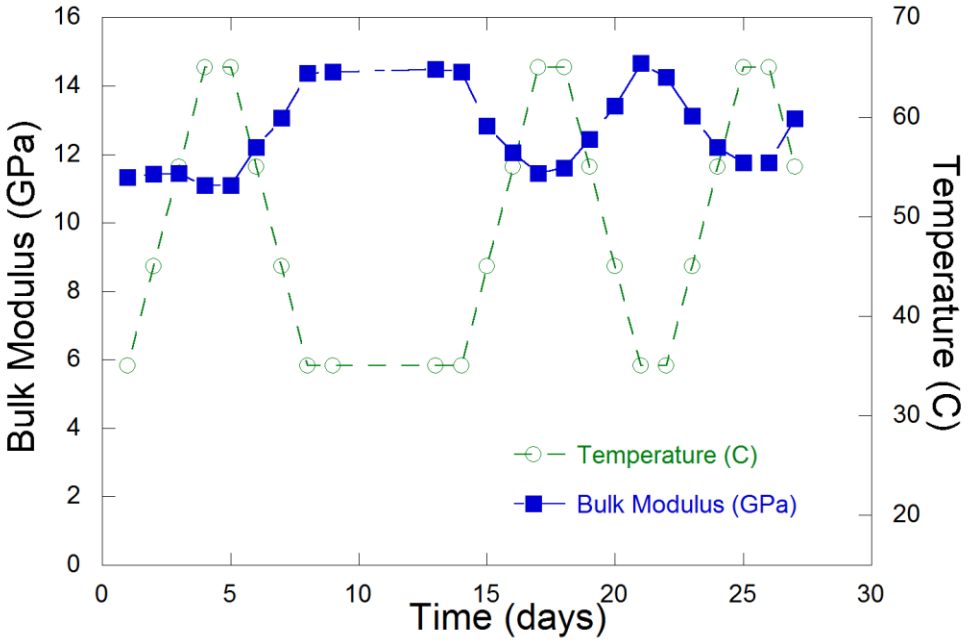

Figure 3.10: Deformation and Temperature vs. Time. There was an unrecovered .1233 mm of deformation (indicated by the solid black double arrow): a 0.47% strain on the sample.

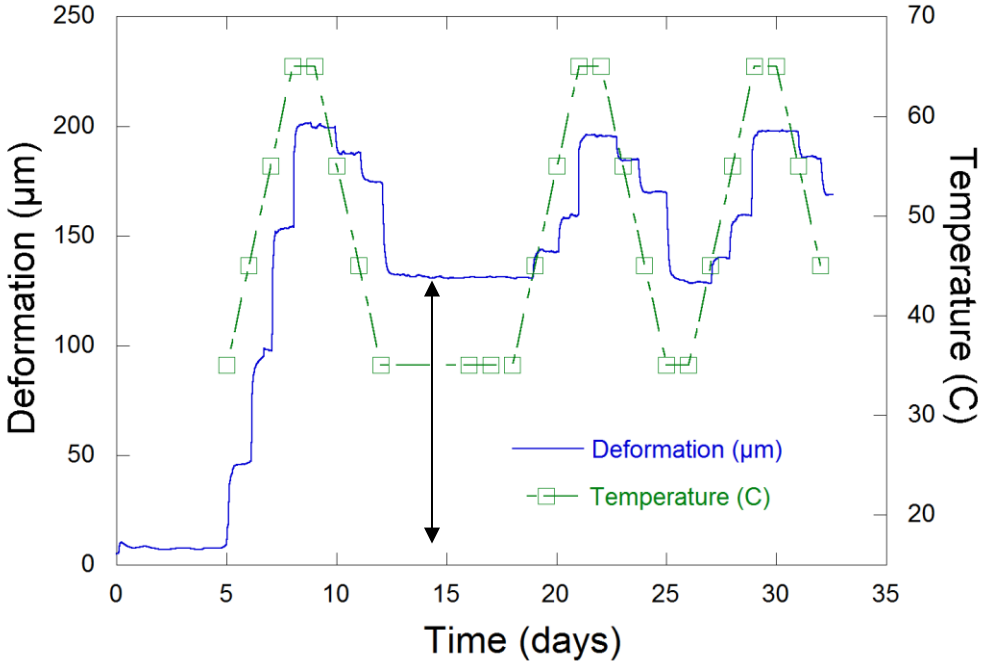

Figure 3.11: Permeability and Bulk Modulus both normalized to a reference measurement.

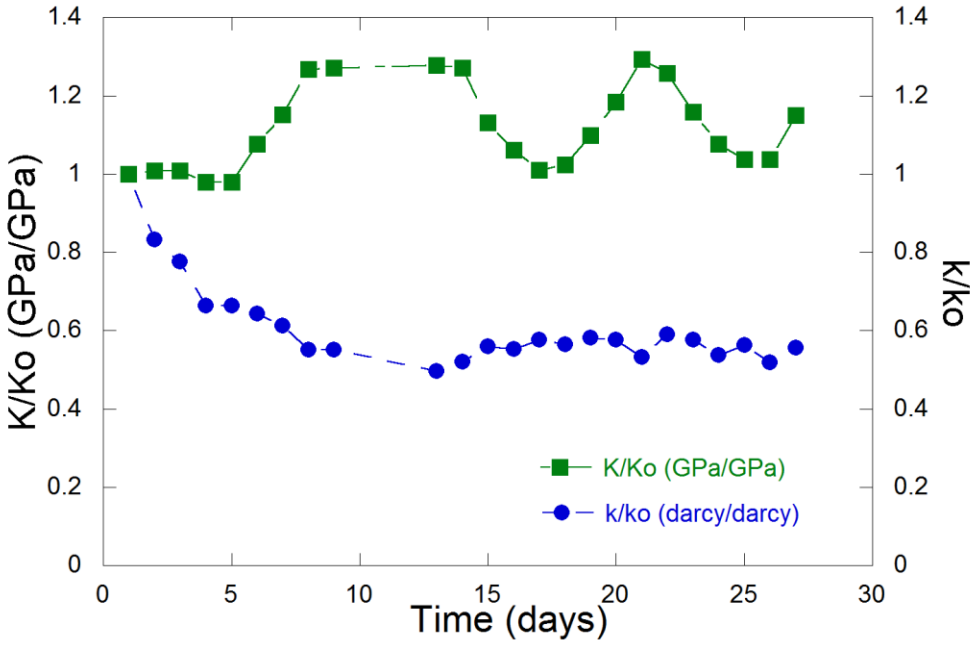

Figure 3.11 shows the relationship between the measured bulk modulus of the sample and the permeability of the sample. There is a general trend where the permeability decreases as the bulk modulus increases, and permeability increases when the bulk modulus decreases. There is hysteresis in both the permeability and the bulk modulus measurements. The permeability is further reduced with each successive cycle and the bulk modulus is further increased with each successive cycle.

The relationship between permeability and bulk modulus is plotted in Figure 3.12. It can be seen that there is a general trend where permeability decreases as the bulk modulus increases. There is notable scatter in the data. Data from the first heating cycle is omitted here, as a separate effect is present in that data.

Each thermal cycle is recorded separately in Figure 3.13, which shows the hysteresis of the bulk modulus with each successive thermal cycle. For the first cycle, the heating phase is characterized by changes that did not occur in the rest of the experiment. Each hysteresis loop starts at a lower measured modulus than it ends, indicative of an additive process occurring during each cycle.

A similar plot of permeability hysteresis loops is presented in Figure 3.14. The first heating cycle shows an initial drop in permeability that is not observed in the remaining two cycles. Permeability exhibits an increasing-neutral trend during temperature increase and a generally decreasing trend during temperature decrease.

Figure 3.12: Permeability vs. Bulk Modulus.

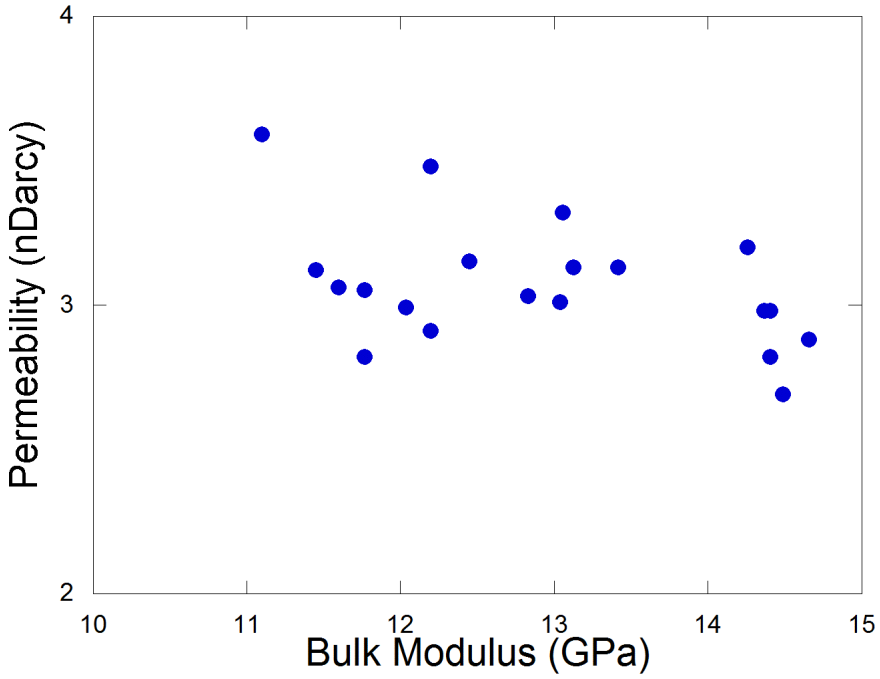

Figure 3.13: Bulk modulus hysteresis loops for three cycles as a function of temperature.

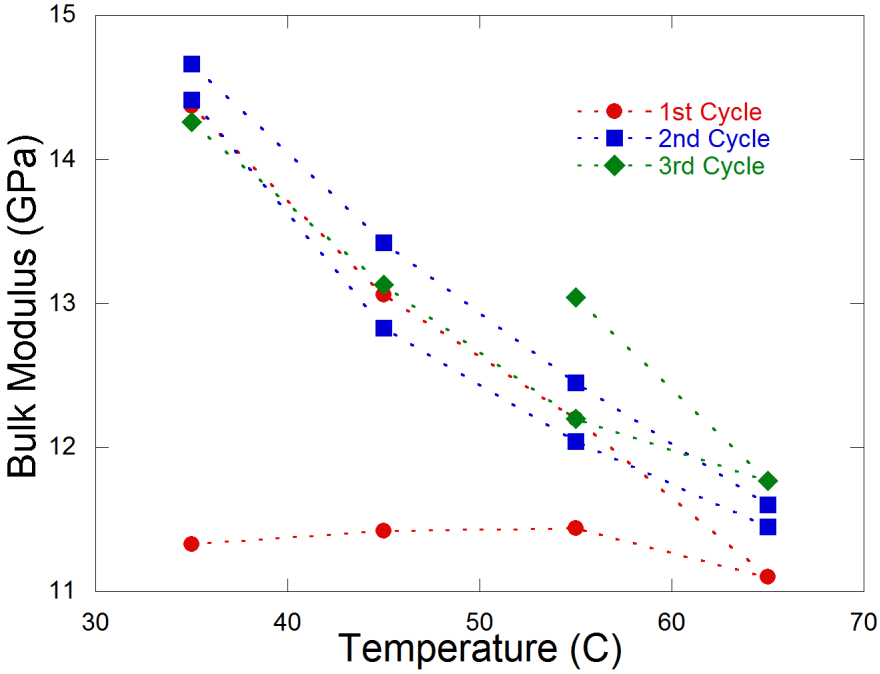

Figure 3.14: Permeability hysteresis loops for three cycles as a function of temperature.

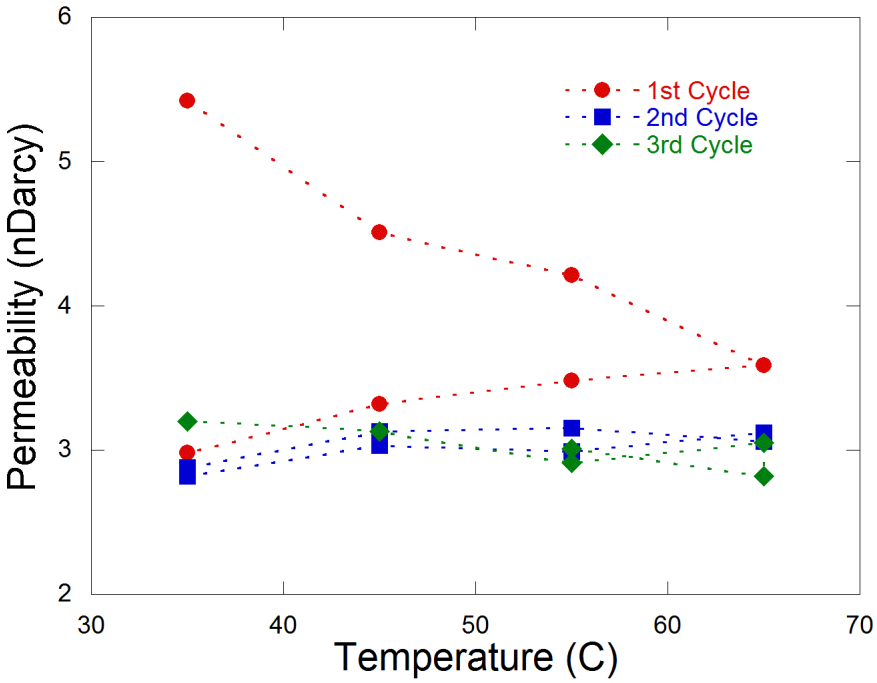

Chapter 4: Discussion

Observations of the evolution of permeability show an inverse linkage between permeability and modulus. We quantify permeability evolution as a function of changing bulk modulus and use this model to examine the response of permeability and bulk modulus to thermal stress. A comparison is made between the contrasting permeability evolution in fractured and unfractured samples and we discuss the implications for flow models in shale. The relationship between rock stiffness and fracture stiffness indicates that fracture compressibility is both non-constant and hysteretic during thermal cycling.

4.1 Permeability Evolution as a Function of Changing Bulk Modulus

In both experiments, the shale samples were cored perpendicular to bedding such that preexisting microfractures were predominantly perpendicular to flow. Longitudinal deformation is largely the result of fracture closure. Longitudinal deformation can be described as

$$u = \frac{\sigma'}{K} L \tag{1}$$

where u is the longitudinal deformation, K is the bulk modulus of the sample, L is the length of the sample, and σ' is the effective stress. The effective stress is

$$\sigma' = \sigma_{ext} - P_p \pm \sigma_{th} \tag{2}$$

where σ_{ext} is the applied external stress, P_p is the pore pressure, and σ_{th} is the thermal stress:

$$\sigma_{th} = E \alpha_{th} \Delta T \tag{3}$$

where E is Young's modulus, α_{th} is the thermal coefficient of expansion for shale, and ΔT represents the change in temperature. Thermal stress is described in (2) as being positive or negative to show that it creates a compressive or tensile stress depending on whether the sample is being heated or cooled, respectively. In (2) the external stress and pore pressure are constant for the second experiment; therefore, the only changing stress is the thermal stress. Changes in permeability can be defined as cubic with changes in aperture:

$$\frac{k}{k_o} = \left(1 + \frac{\Delta b}{b_o}\right)^3 \tag{4}$$

where k is the permeability and is measured in m^2 or nanodarcies, k_o is a reference permeability—in our case taken as the first permeability measurement of a plot, b_o is the aperture of a fracture during the first permeability measurement and Δb is the change in aperture. Because the fractures are predominantly oriented perpendicular to the longitudinal deformation, the majority of deformation will be due to fracture closure, which can then be described as

$$\Delta b = \frac{\Delta u}{L/s} \tag{5}$$

where s is the spacing in between fractures and is an assumed value. A typical value for s would be 10^{-3} m for shales. Therefore b_o can be solved for using the equation

$$k_o = \frac{b_o^3}{12s} \tag{6}$$

which can be rearranged to solve for b_o:

$$b_o = \sqrt[3]{12sk_o} \tag{7}$$

If longitudinal deformation is due to fracture closure, then by (5) Δb can be solved for as

$$\Delta b = \Delta(\frac{\sigma'}{K})s \tag{8}$$

If the changes in thermal stresses are known, the changes in bulk modulus are measured, and the assumption that the change in longitudinal deformation is predominantly due to fracture closure perpendicular to bedding is valid, then (8) can replace the Δb term in (4) to predict changes in permeability such that

$$\frac{k}{k_0} = \left(1 + \Delta\left(\frac{\sigma'}{K}\right)\frac{s}{b_0}\right)^3 \tag{9}$$

Figure 4.1: Comparison of actual and predicted permeability. The R^2 value is 60.3%.

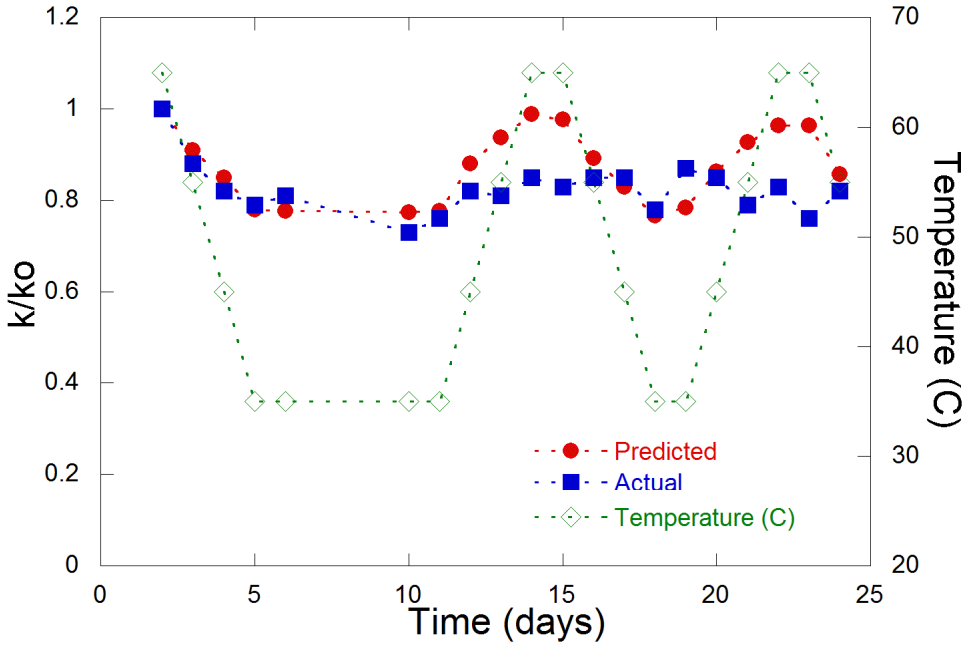

In Figure 4.1 equation (9) captures some of the features present during the thermal cycling experiment. The R^2 value of the points being compared is 60.3%. It is apparent that there were additional mechanisms occurring during each heating phase, in which (9) over predicted the permeability increase. We suggest that this may be due to matrix deformation unrelated to fracture closure, the existence of fractures that are not parallel to bedding, and bridging asperities along fractures that complicate fracture response to thermal stress.

4.2 The Response of Permeability and Bulk Modulus to Thermal Stress

Permeability is enhanced during gas desorption due to fracture dilation (Levine 1996). Increased temperature causes desorption. As shown in Figure 3.3, sorptive strain caused by organic swelling reduces permeability. Our results show that permeability increased at higher temperatures in a fractured sample (Figure 3.6). Fracture dilation was the dominant mechanism for permeability increase and was due in part to desorption. As shown in Figure 3.7, permeability of helium exhibited similar results, indicating that fracture dilation was also caused by mineral expansion along fractures.

Rock stiffness in shales tends to decrease upon heating and increase upon cooling (Closmann 1979, Zhu 2013). Increasing temperature leads to a softening of coals, indicated by a decrease in bulk modulus (Khan 1984). As shown in Figure 3.9, the bulk modulus decreased upon heating and increased upon cooling. It also exhibited hysteretic increase during each thermal cycle (Figure 3.13). Figure 3.8 shows that permeability exhibited the opposite trend. This increase in bulk modulus and decrease in permeability is due to fracture closure. Fracture propagation creates more compliant fractures when the sample returns to a lower temperature. The loss of fracture stiffness causes a loss of fracture aperture, which reduces the permeability.

As shown in Figure 3.10, there was an initial reduction in permeability as the unfractured sample reentered primary consolidation during the first heating cycle. The additional compressive thermal stress increased the effective stress and caused the sample to further consolidate. The complete thermal-stress history of a sample should be known and the sample should be exposed to the full range before experimental data is gathered. Reactivated consolidation was not observed in the fractured shale experiment. Because the permeability of the fractured experiment was three orders of magnitude larger than the permeability recorded during the unfractured sample experiment, the effects of matrix reconsolidation were negligible compared to the more dominant mechanisms through the fracture.

Other investigators have shown experimentally that permeability of intact shale samples decreased with increasing temperature (Sinha 2013). We show that the permeability through a fractured sample increased with increasing temperature (Figure 3.6). Permeability through an unfractured sample decreased during the initial heating phase and increased or remained neutral during subsequent heating phases (Figure 3.8). We suggest that the mechanism responsible for permeability reduction in the work of Sinha is reactivated consolidation.

The mechanism for permeability loss during subsequent cycles is fracture closure during thermal stressing. At low stresses (<30 MPa), there exists a non-linear portion of the stress-strain curve where rocks appear to become stiffer as pre-existing cracks and pores close (Walsh 1966, Scholz

1968). Stress-strain curves for coal have a similar non-linear portion at low stress due to closing of pre-existing cleats in the coal that correlates with permeability reduction (Wang 2013).

4.3 Implications for Fracture Compressibility during Thermal Cycling

Assuming constant pore volume compressibility is reasonable for many coal basins (McKee 1987). Such an assumption leads to erroneous estimates in other basins (Palmer 2009). Our results indicate that this assumption would no longer be valid if thermal cycling were implemented. During thermal cycling, changes in the pore volume compressibility are large, which is seen in the increase in fracture compliance during thermal unloading.

Growth of preexisting fractures leads to greater fracture compliance and an increase in bulk modulus upon cooling. Therefore during temperature cycling the propagation of preexisting fractures leads to a loss of fracture stiffness, a loss of fracture aperture, a loss of permeability, and an increase in bulk modulus. Until fractures begin to coalesce, permeability would not permanently increase.

Chapter 5: Conclusion

Cycled thermal stresses applied to both fractured and unfractured samples of shale result in similar permeability trends. Bulk modulus decreased while permeability increased or remained neutral with increasing temperature, whereas the opposite trend was observed with decreasing temperature. Both permeability and bulk modulus exhibited a hysteretic response to cycling. Thermal stresses can reactivate primary consolidation, but additional cycling may dampen this effect. A proposed model defines permeability evolution as an inverse function of changes in bulk modulus. This model captures the essential effects of thermal cycling, but the existence of other mechanisms is apparent. Other mechanisms may include matrix deformation unrelated to fracture closure, the existence of fractures that are not parallel to bedding, and bridging asperities along fractures that complicate fracture response to thermal stress. Results are summarized below:

1. Permeability evolution of a fractured sample is similar to that of an unfractured sample.
2. Heating can cause primary consolidation to be reactivated and permeability to be reduced.
3. Heating causes a temporary increase in permeability due to mineral expansion along fractures.
4. Thermal cycling leads to a loss of fracture stiffness, an increase in bulk modulus, and a decrease in permeability due to reduced aperture.
5. Thermal cycling causes additive damage by way of propagation of preexisting microfractures. This is seen in the hysteretic nonlinear response of permeability and bulk modulus.

It is concluded that thermal cycling leads to a permeability reduction in shales. However, it is noted that with large enough tensile thermal stresses or after applying additional cycles, microfractures would begin to coalesce leading to permeability enhancement. For the application of shale gas production, this can lead to an improved ultimate recovery.

References

Brace, W. F., J. B. Walsh, and W. T. Frangos. "Permeability of granite under high pressure." *Journal of Geophysical Research* 73.6 (1968): 2225-2236.

Chen, Z., et al. "Effect of the effective stress coefficient and sorption-induced strain on the evolution of coal permeability: experimental observations." *International Journal of Greenhouse Gas Control* 5.5 (2011): 1284-1293.

Closmann, P. J., and W. B. Bradley. "The effect of temperature on tensile and compressive strengths and Young's modulus of oil shale." *Society of Petroleum Engineers Journal* 19.05 (1979): 301-312.

Costin, L. S. "A microcrack model for the deformation and failure of brittle rock." *Journal of Geophysical Research: Solid Earth* 88.B11 (1983): 9485-9492.

Cui, X., and R. M. Bustin. "Volumetric strain associated with methane desorption and its impact on coalbed gas production from deep coal seams."*AAPG Bulletin* 89.9 (2005): 1181-1202.

Eberhardt, E., D. Stead, and B. Stimpson. "Quantifying progressive pre-peak brittle fracture damage in rock during uniaxial compression." *International Journal of Rock Mechanics and Mining Sciences* 36.3 (1999): 361-380.

Faoro, I., et al. "Linking permeability to crack density evolution in thermally stressed rocks under cyclic loading." *Geophysical Research Letters* 40.11 (2013): 2590-2595.

Izadi, G., et al. "Permeability evolution of fluid-infiltrated coal containing discrete fractures." *International Journal of Coal Geology* 85.2 (2011): 202-211.

Jasinge, D., P. G. Ranjith, and S. K. Choi. "Effects of effective stress changes on permeability of latrobe valley brown coal." *Fuel* 90.3 (2011): 1292-1300.

Khan, M. R., and R. G. Jenkins. "Thermoplastic properties of coal at elevated pressures: 1. Evaluation of a high-pressure microdilatometer." *Fuel* 63.1 (1984): 109-115.

Kumar, H., et al. "Permeability evolution in sorbing media: analogies between organic- rich shale and coal." *Geofluids* (2015).

Levine, J. R. "Model study of the influence of matrix shrinkage on absolute permeability of coal bed reservoirs." *Geological Society, London, Special Publications* 109.1 (1996): 197-212.

Liu, H., and J. Rutqvist. "A new coal-permeability model: internal swelling stress and fracture–matrix interaction." *Transport in Porous Media* 82.1 (2010): 157-171.

Liu, J., et al. "Linking gas-sorption induced changes in coal permeability to directional strains through a modulus reduction ratio." *International Journal of Coal Geology* 83.1 (2010): 21-30.

Liu, J., et al. "Interactions of multiple processes during CBM extraction: a critical review." *International Journal of Coal Geology* 87.3 (2011): 175-189.

McKee, C. R., A. C. Bumb, and R. A. Koenig. "Stress-dependent permeability and porosity of coal." *International Coalbed Methane Symposium, University of Alabama, Tuscaloosa, Alabama* Nov 16 (1987): 183-193.

Palmer, I., and J. Mansoori. "How Permeability Depends on Stress and Pore Pressure in Coalbeds: A New Model." *SPE Reservoir Evaluation & Engineering* (1998).

Palmer, I. "Permeability changes in coal: analytical modeling." *International Journal of Coal Geology* 77.1 (2009): 119-126.

Pekot, L. J., and S. R. Reeves. "Modeling the effects of matrix shrinkage and differential swelling on coalbed methane recovery and carbon sequestration." *Paper 0328, proc. 2003 International Coalbed Methane Symposium. University of Alabama*. 2003.

Robertson, E. P., and R. L. Christiansen. "A permeability model for coal and other fractured, sorptive-elastic media." *SPE Journal* 13.03 (2008): 314-324.

Rybacki, E., T. Meier, and G. Dresen. "What controls the mechanical properties of shale rocks?–Part II: Brittleness." *Journal of Petroleum Science and Engineering* 144 (2016): 39-58.

Scholz, C. H. "Microfracturing and the inelastic deformation of rock in compression." *Journal of Geophysical Research* 73.4 (1968): 1417-1432.

Shi, J., and S. Durucan. "A model for changes in coalbed permeability during primary and enhanced methane recovery." *SPE Reservoir Evaluation & Engineering* 8.04 (2005): 291-299.

Sinha, S., et al. "Steady-state permeability measurements on intact shale samples at reservoir conditions-effect of stress, temperature, pressure, and type of gas" *SPE Middle East Oil and Gas Show and Conference*. Society of Petroleum Engineers, 2013.

Walsh, J. B., and W. F. Brace. "Elasticity of rock: A review of some recent theoretical studies." *Rock Mechanics and Engineering Geology* 4.4 (1966): 283-297.

Wang, S., D. Elsworth, and J. Liu. "A mechanistic model for permeability evolution in fractured sorbing media." *Journal of Geophysical Research: Solid Earth* 117.B6 (2012).

Wang, S., D. Elsworth, and J. Liu. "Permeability evolution during progressive deformation of intact coal and implications for instability in underground coal seams." *International Journal of Rock Mechanics and Mining Sciences* 58 (2013): 34-45.

Wu, Y., et al. "Evolution of coal permeability: Contribution of heterogeneous swelling processes." *International Journal of Coal Geology* 88.2 (2011): 152-162.

Yin, G., et al. "Combined effect of stress, pore pressure and temperature on methane permeability in anthracite coal: an experimental study." *Transport in Porous Media* 100.1 (2013): 1-16.

Zhu, C., and C. Arson. "A thermo-mechanical damage model for rock stiffness during anisotropic crack opening and closure." *ACTA Geotechnica* 9.5 (2014): 847-867.